ACS APPLIED MATERIALS & INTERFACES

Research Article

www.acsami.org

Azobenzene-Functionalized Gold Nanoparticles as Hybrid Double-Floating-Gate in Pentacene Thin-Film Transistors/Memories with Enhanced Response, Retention, and Memory Windows

Chiao-Wei Tseng,[†] Ding-Chi Huang,[‡] and Yu-Tai Tao*[,†,‡]

[†]Institute of Chemistry, Academia Sinica, Taipei, Taiwan

[‡]Department of Chemistry, National Tsing-Hua University, Hsin-chu, Taiwan

Supporting Information

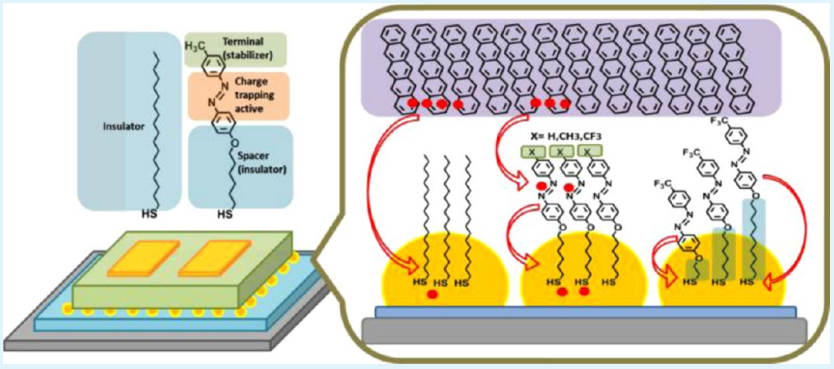

ABSTRACT: Gold nanoparticles (Au-NPs) with surfaces covered with a self-assembled monolayer of azobenzene derivatives were prepared at the interface of dielectric insulator SiO_2 and pentacene thin film. Transistors constructed with these composite channel materials exhibited electric bistability upon different gate biases, with the monolayer serving as a barrier layer, a work function modulator, as well as additional charge trapping sites at the Au-NPs/semiconductor interface at the same time. In comparison with simple alkanethiol monolayer-covered Au-NPs, the CH_3-substituted azobenzene-functionalized Au-NPs result in a transistor memory device with about 70% more charges trapped, much faster response time as well as higher retention time. Besides, depending on the substituent on the azobenzene moieties (CH_3, H, or CF_3) and the tethering alkyl chain length, the speed at which the carriers are trapped (affecting switching response) and the stability of the carriers that are trapped (affecting memory retention) can be modulated to improve the device performance. The structural characterization and electronic characteristics of these devices will be detailed.

KEYWORDS: *organic field-effect transistors, organic memory devices, double-floating gate, self-assembled monolayer, gold nanoparticles*

1. INTRODUCTION

Field-effect transistors based on organic semiconductors as the conducting channel have reached a state such that replacing the traditional inorganic counter parts in electronics is both attractive and practical, due to the improvement in the mobility in recent years.[1−4] Memory device based on organic material for data storage is yet another important component to consider in electronic circuitry.[5−7] The generic questions to ask in a nonvolatile memory device are: how fast is the switching between the on/off states (response time), how long will the on/off state last (retention time) and how large is the memory window. Incorporating memory function to a transistor is also attracting much interest.[8−10] This has been achieved by intentionally incorporating charge carrier traps,[11−13] or polymer electrets,[14−16] or ferroelectric polymers[17−19] in the conducting channel and in the dielectric layer respectively to effect conductivity changes upon some switching action such as application of a bias or photoirradiation. The use of metal nanoparticles surrounded and/or embedded in the channel materials instead of using traditional planar floating gates has the advantage of maximizing contact between charge trapping sites and the organic semiconductor and minimizing the charge leakage because all sites are independent and isolated.[20−22] An insulating coating, either in the form of a molecular layer, or the metal oxide, is needed to keep the charges in the particles during the programming/erasing process.[23−25] However, the same film needed to retain the charges (leading to memory retention) could also be a barrier for the charges to be trapped (affecting the response time). Thus merely increasing the thickness of the insulating layer increases charge retention time but slows down the response speed (programming/erasing speed) at the same time, although a fast response and an

Received: June 17, 2013
Accepted: September 11, 2013
Published: September 11, 2013

   dx.doi.org/10.1021/am4023253 | ACS Appl. Mater. Interfaces 2013, 5, 9528−9536

extended retention are more desirable. The amount of charges that can be trapped at the trapping sites in turn determines the extent of threshold voltage shift (thus the width of the memory window). A careful design of the device structure is needed to address all these interrelated issues.

The photoinduced isomerization of azobenzene dyes has been widely used as switches in some mechanical[26,27] and electronic applications.[28,29] The incorporation of azobenzene moieties in a dielectric layer has also been used in fabricating memory devices due to the dipole change upon photoisomerization.[30,31] Nevertheless, the threshold voltage shifts and the on/off ratio involved are in general small. In this work, we demonstrated that by using gold nanoparticles capped with a monolayer of azobenzene derivatives as the charge trapping moieties in the conduction channel of a pentacene thin film transistor, memory device with fast response, long retention, and large memory window can be achieved. Both the particle itself and the monolayer on the surface can trap charge carriers. The particle body provides the reservoir for charge carriers, whereas the azobenzene moieties at the surface mediate and stabilize the specific charges that can transfer from pentacene to the Au-NPs, through appropriate choice of the substituent at the azobenzene moieties. This leads to a much enhanced switching response and charge retention versus the otherwise a passive and insulating monolayer of alkyl chains.

2. EXPERIMENTAL SECTION

Materials. *n*-Octadecanethiol (C18SH) and *n*-decanethiol (C10SH) were obtained commercially. All azobenzene-carrying thiols (structures and corresponding abbreviations shown in Figure 1) were

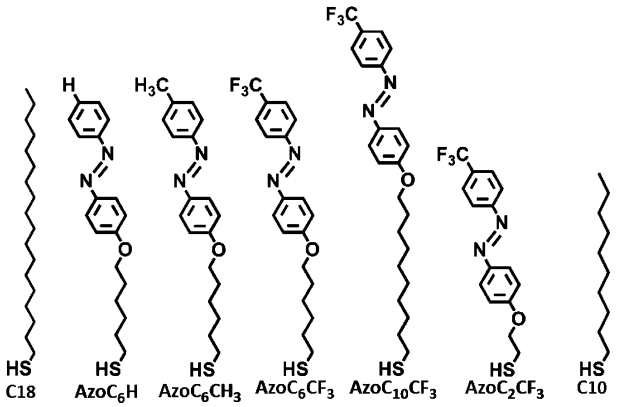

Figure 1. Monolayer-forming thiols used in this study.

synthesized in the laboratory and fully characterized by ^{1}H NMR, and ^{13}C NMR, spectrometry (see the Supporting Information). Pentacene was purchased from Aldrich and was purified by subliming twice through a temperature-gradient sublimator. Gold metal (99.99% purity) was obtained from Elecmat Inc. USA.

The highest occupied molecular orbital (HOMO) and lowest unoccupied molecular orbital (LUMO) levels of various azobenzene derivatives were determined by cyclic voltammetry and UV absorption edge method as described before.[32]

Device Fabrication and Characterization. The pentacene-based FETs were fabricated by physical vapor deposition (in a vacuum of 2×10^{-5} Torr at a deposition rate of 0.2 Å/s) of 60 nm pentacene film on an n-type silicon (100) substrate (the gate electrode), which was covered with a 300-nm thick, thermally grown oxide layer as the insulating dielectric. Source and drain electrodes were deposited through a shadow mask to achieve a top-contact FET configuration with a channel length of 50 μm and channel width of 500 μm. For the Au-NPs-embedded pentacene films, the oxide-covered silicon substrate (SiO_2) was first treated with 3-mercaptopropyltrimethoxysilane, which served as the adhesion layer for Au-NPs. Au-NPs were prepared by thermally depositing 4 nm gold at a rate of 0.1 Å/s on the surface. Discrete Au particles with an average diameter of 21 nm were obtained according to the histogram analysis (see the Supporting Information, Figure S1). Additional cleaning by low-power oxygen plasma for 5 min was carried out to clean off both the SiO_2 and the Au-NPs surfaces. Self-assembled monolayers on Au-NPs were formed by immersing these nanoparticle-decorated substrates immediately in a 1 mM THF solution of thiol molecules for 12 h, followed by a thorough rinse with pure THF before the pentacene film deposition.

Planar gold samples were prepared in parallel for some of the physical and spectroscopic characterizations of the adsorbed monolayers on Au surface. Thus the reflectance infrared spectra were recorded with a Varian 640-IR spectrometer equipped with a MCT detector at a 4 cm^{-1} resolution at room temperature. The thickness of thiol-monolayers was measured by ellipsometer. Contact angle was measured by the DIGIDROP GBX contact angle meter using ultrapure water as the wetting liquid. UV-irradiation of the film samples was delivered by a UV lamp (365 nm wavelength) with an intensity of 4 mW/cm^2 held at 3 cm distance from the sample under ambient condition.

Atomic force microscopy analyses were carried out with a Multimode Atomic Force Microscope (Digital Instruments, Nanoscope III) using tapping mode with a silicon tip. The powder X-ray diffraction measurements were carried out with a Philips X'Pert diffractometer equipped with an X'Celerator detector. The electrical characteristics of the transistor devices were measured in ambient with a HP4156 parameter analyzer.

3. RESULTS AND DISCUSSION

3.1. Characterization of the Surface Films. The Au-NPs prepared by thermally evaporating 4 nm pure gold metal onto the silica substrate were discrete and nonconnected, giving a substrate as nonconductive as the silica substrate itself. Plasma cleaning of the surbtrate and then the SAM formation on the Au-NPs had little effect on the particle sizes and morphology. The azobenzene moieties were tethered to the gold particle surface through a mercaptoalkyloxy group, with the para substituent and the alkyl chain length as the variables (abbreviated as AzoCnX, where the "X" stands for the p-substituent and "*n*" the number of carbon in the alkyl chain). The structures and corresponding abbreviations of all azobenzene-carrying thiols are shown in Figure 1. Adsorption of various azobenzene-containing thiols on a planar gold surface was carried out in parallel as the control samples for monolayer formation and analysis. Ellipsometry and the reflection–absorption infrared spectroscopy (RAIRS) on planar Au substrates confirmed the presence of a monolayer (see Figure S2 in the Supporting Information). Water contact angles were measured for various SAM-modified surfaces and hydrophobic character ($\theta(H_2O) > 90°$) were obtained in all cases. Adsorption of various azobenzene thiols also changed the work function of Au surface. A high work function of about 6.0 eV was observed for $AzoC_6CF_3$-covered surface. Whereas, similar work function of about 4.5 and 4.7 eV was obtained for *n*-alkyl thiols (C10 and C18) and $AzoC_6CH_3$-covered surface. The variation of work function is presumably due to the direction of oriented dipole formed at the surface.[33,34] All the data are summarized in Table 1.

Pentacene films deposited at a substrate temperature of 24 °C were characterized by X-ray diffraction and AFM microscopy. The X-ray diffraction patterns for pentacene films on silica substrates decorated with various thiol-modified Au-NPs are shown in Figure 2. The thin film phase of

Table 1. Film Thicknesses, Contact Angles and Work Functions of SAM-Modified Au Surfaces

SAM-Au	thickness (nm)	water contact angle (deg)	work function (eV)
C18-Au	2.1	109.6	4.5
$AzoC_6H$-Au	2.0	91.8	4.9
$AzoC_6CH_3$-Au	2.0	101.6	4.7
$AzoC_6CF_3$-Au	2.1	100.2	6.0
$AzoC_{10}CF_3$-Au	2.6	101.8	6.0
$AzoC_2CF_3$-Au	1.4	99.6	5.9
C10-Au	1.2	107.1	4.5

pentacene film with the diffraction planes of (001), (002), (003), and (004) was observed on all substrates.[35]

Pentacene film deposited on surface with C18SH-modified Au-NPs has the highest intensity of the diffraction peaks, reflecting a better crystallinity of the film deposited. The peak intensity strongly depended on the terminal functional group for the azobenzene-covered surfaces, which may be attributed to different surface energy[36,37] The morphologies of the pentacene films on various surfaces are shown in Figure 3. The pentacene film deposited on the substrate with C18-Au-NPs apparently exhibited larger grain size, ranging from 0.2 to 1 μm in diameter. The grain size changed with the terminal groups as well. It is suggested that the SAMs of *n*-alkanethiol generate an outer surface of lower energy due to the nonpolar methyl terminal groups. For azobenzene-SAM, CF_3-substitued ones yield surfaces of lower energy, and thus, the $AzoC_6CF_3$-Au-NPs led to pentacene films of higher crystallinity and large grain sizes. With decreasing chain length of the azobenzene-SAM, only a small difference in the grain sizes and crystallinity of the pentacene films was observed (Figure 2b). This is also reflected by the higher water contact angles for the planar control samples with similar modification (Table 1).

3.2. Electrical Properties. Thin film transistors of top-contact, bottom-gate configuration with pentacene films embedding various SAM-modified Au-NPs as the channel materials were fabricated and the electric property measured. As the gate bias was swept from +80 to −80 V, the source-drain current increased with increasingly negative gate bias after a threshold voltage, which is typical for p-channel devices (see Figure S3 in the Supporting Information). The field-effect carrier mobility (Table 2) apparently depended on the crystallinity of the pentacene film, which was reflected by the X-ray and AFM results. An apparent, repeatable threshold voltage shift (or hysteresis) of the transfer current was observed in the bisweeps of gate bias. This is attributed to the charge trapping effect of Au-NPs because the reference devices without the Au-NPs along the channel had little of such hysteresis.[37] The Au-NPs served as the floating gate in the transistor device.[38,39] Upon an external gate bias, the charge carriers from channel region were trapped into the floating gate (programming process). The formation of an internal electric field by the trapped charges in the floating gate partially offseted or enhanced the external applied gate bias and thus could be used to manipulate the threshold voltage (V_{th}) and the channel conductance of the device. The trapped charge carriers would be detrapped back to the channel upon a reverse gate bias (erasing operation). The memory window (or the hysteresis width), defined as the threshold voltage shift (ΔV_{th}) between the forward and reverse sweep of gate bias, signifies the ability of charge storage in the NPs. Apparently, the memory window changed with the monolayer used in capping the Au-NPs (Figure 4). The data were further analyzed as follows.

3.2.1. Effect of Azobenzene Moieties. Previous studies showed that the surface treatment of the Au-NPs (the floating gate) with *n*-alkanethiol or fluorinated *n*-alkanethiol monolayer plays a critical role in affecting the efficiency of charge trapping due to the insulating chain length (tunneling distance) imposed and the work function modulation (energy level alignment) caused by the direction of dipole moment of the modifying layer, thus a dependence of the hysteresis width on the chain length and type of alkyl chain (hydrocarbon or fluorinated chain) was observed.[23,37] When comparing the IV hysteresis of the devices with the C18-modified and the $AzoC_6CH_3$-modified Au-NPs in the present case, one noticed that devices with $AzoC_6CH_3$-Au-NPs possessed a much larger memory window (Figure 4 and Table 2).

The C18 monolayer and $AzoC_6CH_3$ monolayer have similar molecular length, and the same dipole direction. The work functions of Au substrates covered with the two types of monolayer are also similar (4.5 and 4.7 eV respectively, Table 1). The larger memory window observed can be attributed to the additional charge trapping sites provided by the azobenzene moieties, as well as the mediating effect of the azobenzene-layer in charge transfer to the Au-NPs, as will be explained later. The amount of trapped charges at the interface can be estimated according to eq 1[40]

$$\Delta V_{th} = -\frac{d_i Q}{\varepsilon_i} = -\frac{Q}{C_i} \quad (1)$$

Where C_i is the dielectric capacitance and ΔV_{th} is the shifts of the threshold voltage. For the $AzoC_6CH_3$-Au-NP device, which yielded a memory window of 94.3 V, the total density of charge carriers trapped is calculated to be 6.8×10^{12} cm^{-2}, based on a C_i = 11.5 nF cm^{-2}. Compared to the density of Au-NPs ($2.8 \times$

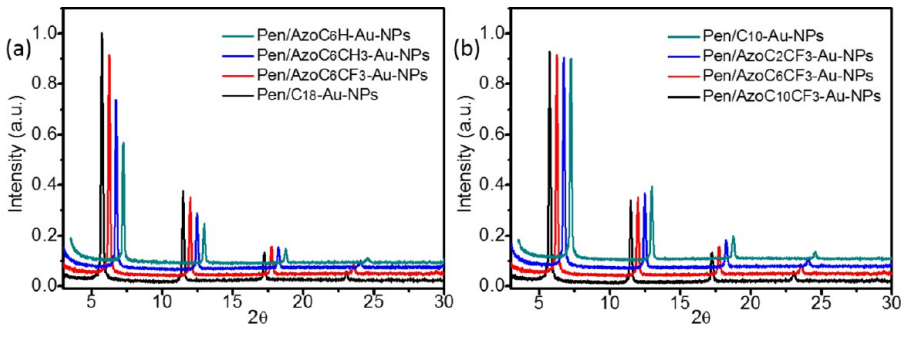

Figure 2. X-ray diffraction patterns of pentacene films deposited on various azobenzene- and *n*-alkane-monolayer-covered Au-NPs/silica surfaces.

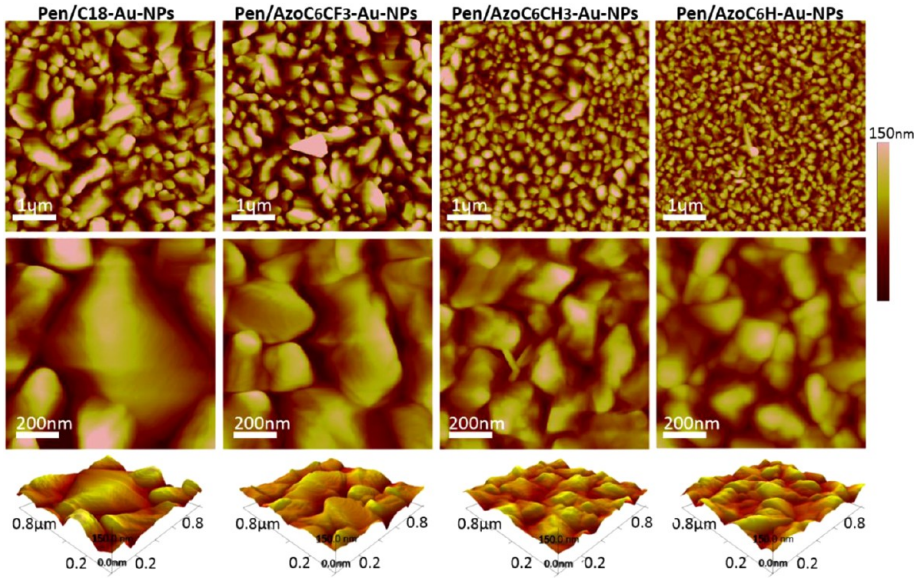

Figure 3. AFM images of pentacene films deposited on *n*-octadecanethiol and various azobenzene thiol monolayer-covered Au-NPs/silica substrates.

Table 2. Device Characteristics As a Function of Surface Modification of Au NPs

SAM-Au-NPs	threshold voltage (V_{th}) (V)	mobility ($\times 10^{-3}$)	on−off ratio	memory window (V)	retention (s)
C18-Au-NPs[a]	28.0	4.1	1×10^3	54.9	10^6
AzoC6H-Au-NPs[a]	64.1	0.2	1×10^2	102.5	10^3
AzoC6CH3-Au-NPs[a]	58.1	0.7	1×10^3	94.3	10^7
AzoC6CF3-Au-NPs[a]	42.0	1.4	1×10^2	50.3	10^6
AzoC10CF3-Au-NPs[b]	98.8	0.5	1×10^2	18.9	10^8
AzoC6CF3-Au-NPs[b]	61.3	1.2	1×10^3	60.8	10^6
AzoC2CF3-Au-NPs[b]	80.7	3.3	1×10^3	80.5	10^5
C10-Au-NPs[b]	55.7	1.6	1×10^2	86.0	10^3

[a]The gate bias was applied between 80 and −80 V. [b]The gate bias was applied between 100 and −100 V.

10^{11} NP cm^{-2}, roughly estimated from AFM images), around 24 charge carriers were trapped in each Au-NP. This is ∼70% more charges trapped than the device with C18-Au-NP device, which is estimated to have 14 trapped charges per Au-NP. That a monolayer of $AzoC_6CH_3$ molecules on a planar dielectric substrate can store charges under gate bias was demonstrated previously.[41] The program/erase speed, which refers to the switching response of the devices, can be seen in the plot of current (I_{DS}) as a function of gate pulse time (Figure 5a). Upon an applied +100 V and −100 V gate pulse respectively, the $AzoC_6CH_3$-Au-NP devices reached the maximum current (ON state) and minimum current (OFF state) quicker, especially for the minimum current, in about 60 and 0.01 s, respectively. In contrast, for the C18-Au-NP system, the current changed steadily and did not yet reached the maximum current or the minimum current even after 180 s pulse. The fast trapping speed of charges results in more charges in the nanoparticles with the same bias pulse. A higher ON/OFF ratio is also obtained.

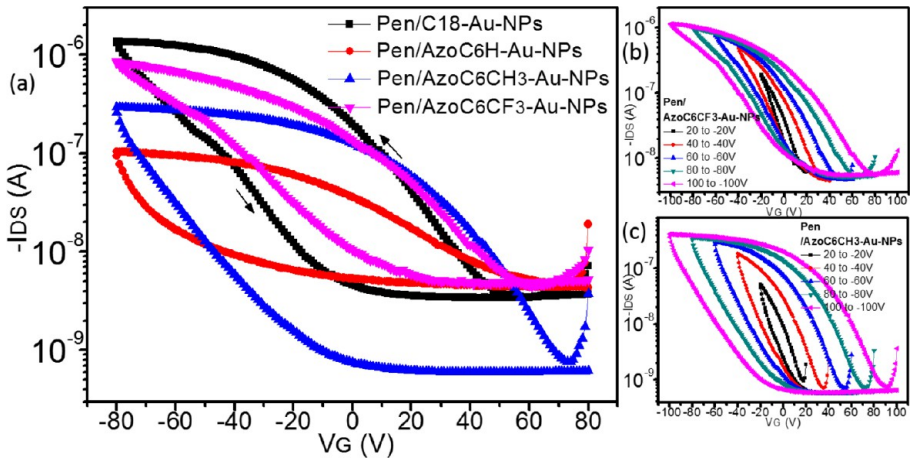

Figure 4. (a) Transfer characteristics of bidirection scans for devices with various SAM-modified Au-NPs substrates. The V_{ds} was kept at −50 V and the V_{gs} bias was swept from +80 to −80 V and returned to +80 V again; (b, c) transfer characteristics as a function of scan ranges of the gate bias for the devices with $AzoC_6CF_3$- and $AzoC_6CH_3$-Au-NPs surfaces, respectively.

dx.doi.org/10.1021/am4023253 | ACS Appl. Mater. Interfaces 2013, 5, 9528−9536

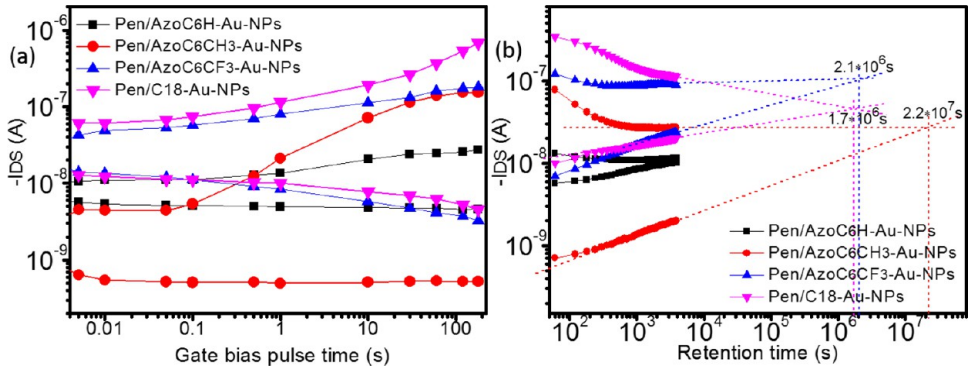

Figure 5. (a) Source−drain current as a function of gate pulse time for devices with $AzoC_6H$-Au-NPs, $AzoC_6CH_3$-Au-NPs, $AzoC_6CF_3$-Au-NPs, and C18-Au-NPs, respectively. (b) Retention characteristics of the corresponding devices with $AzoC_6H$-, $AzoC_6CH_3$-, $AzoC_6CF_3$-, and C18-Au-NPs, respectively.

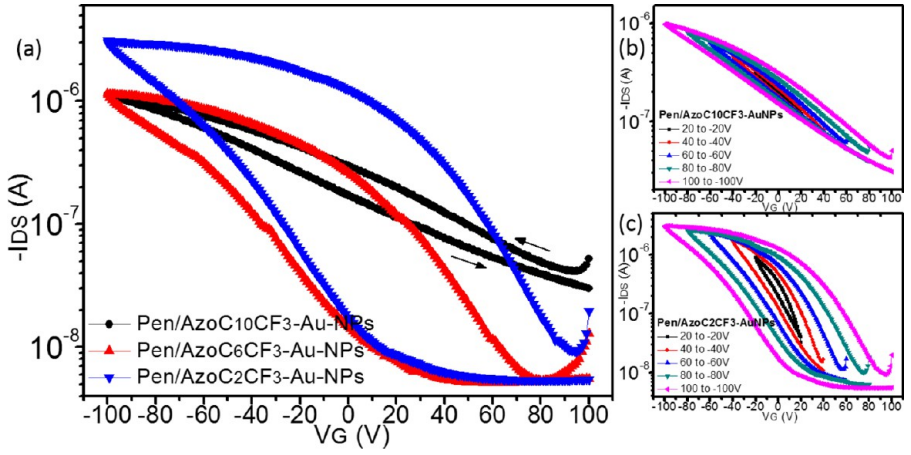

Figure 6. (a) Transfer characteristics of bidirection scans of the $AzoC_{10}CF_3$, $AzoC_6CF_3$, and $AzoC_2CF_3$-covered Au-NP devices, respectively. The V_{ds} was kept at −50 V and the V_{gs} bias was swept from +80 to −80 V and returned to +80 V again; (b, c) transfer characteristics as a function of scan ranges of the gate bias for the devices with $AzoC_{10}CF_3$- and $AzoC_2CF_3$-covered Au-NPs surfaces, respectively.

The charge retention characteristics, reflecting the capability of the NPs in holding the charges within the particles, was measured by recording the current with time in the absence of gate bias after the application of −100 V/+100 V gate pulses at 24 °C in air (Figure 5b). The $AzoC_6CH_3$-Au-NP device shows a longer retention time compared with the C18-Au-NP device. By extrapolating the current plot, the time for the ON/OFF currents approaching each other is estimated to be around 1×10^6 s for the C18-Au-NP device and 1×10^7 s for the $AzoC_6CH_3$-Au-NP device, thus an order of magnitude improvement. The rationale for the fast response and longer retention for $AzoC_6CH_3$-Au-NP device will also be discussed later.

3.2.2. Effect of Substituent on the Azobenzene Moiety. The substituent influences the work function of the metal due to the direction of the dipole moment associated with the substituted molecules in the oriented monolayer.[33,34] Thus the monolayers of $AzoC_6H$ and $AzoC_6CH_3$ lower the work function of Au substrate and decrease the Schottky barrier for hole carriers to transfer from pentacene to Au-NPs, making the transport easier. In contrast, the $AzoC_6CF_3$-modified Au substrate has a higher work function and makes the hole charge transport to Au-NPs harder. A comparison of the IV hysteresis of the devices incorporating Au-NPs covered with differently substituted azobenzenes (Figure 4a) shows that the memory window increases in the order of $AzoC_6CF_3$ < $AzoC_6H$ < $AzoC_6CH_3$, in agreement with the expectation that lower work function favors hole carrier transfer to the NPs. Furthermore, the switching speed of the device, reflected by the time it takes to reach the "ON" or "OFF" state, also shows a dependence on the substituent: the $AzoC_6CH_3$ system reached the minimum current state ("OFF" state) in 0.01 s, whereas the $AzoC_6H$ system reached the minimum current in 0.1 s. Yet the $AzoC_6CF_3$ system did not reach the minimum current after 100 s, upon the same gate bias pulse of −100 V. All three systems reached the maximum current (ON state) slower, but the $AzoC_6CH_3$ had the steepest increase of current and the $AzoC_6CF_3$ has the smallest increase (Figure 5a). When the gate bias was turned off after the initial pulses, the "ON" current decreased gradually, with the $AzoC_6CH_3$ system decreased the fastest initially and then stabilized. On the other hand, the "OFF" current increased slowly. By extrapolating the ON and OFF currents, it is seen the $AzoC_6CH_3$-Au-NPs system has a longer retention time (~2×10^8 s) than the $AzoC_6CF_3$-Au-NP system (~2×10^7 s), with the $AzoC_6H$-Au-NPs system giving the shortest retention (~5×10^3 s) (Figure 5b).

The magnitude of the shifts of threshold voltage (memory window) as a function of gate bias sweeping range was also examined (Figure 4b, c). Increasing the sweeping range of the gate bias increased the threshold voltage shifts, presumably because more charges were being accumulated at the interface and got trapped at higher gate bias. The threshold voltages shift

dx.doi.org/10.1021/am4023253 | ACS Appl. Mater. Interfaces 2013, 5, 9528−9536

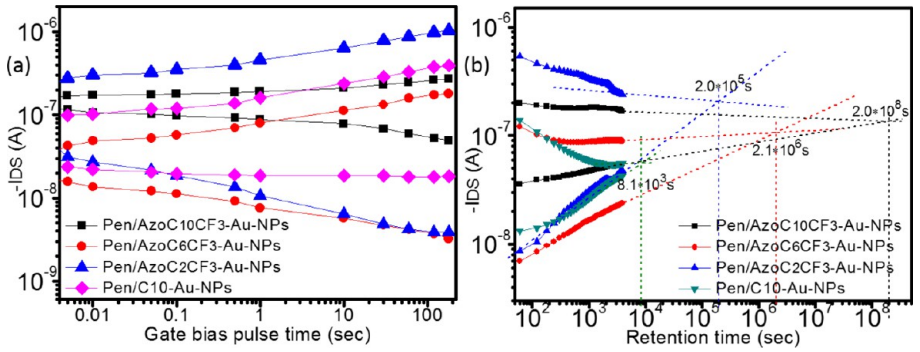

Figure 7. (a) Source−drain current as a function of gate pulse time for devices with $AzoC_{10}CF_3$-Au-NPs, $AzoC_6CF_3$-Au-NPs, $AzoC_2CF_3$-Au-NPs and C10-Au-NPs, respectively. (b) Retention characteristics of the corresponding devices.

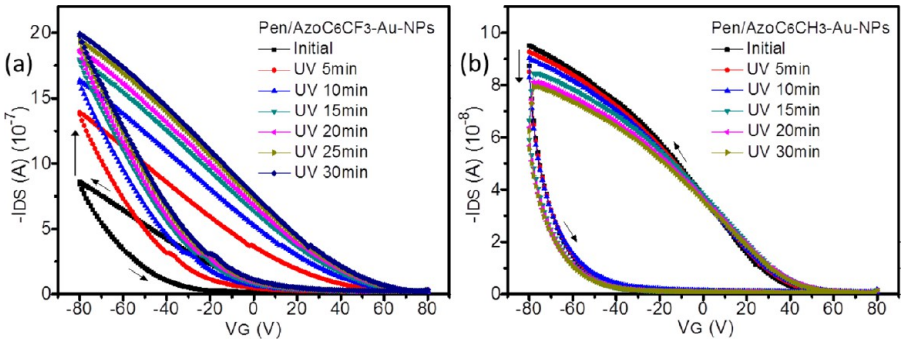

Figure 8. Transfer characteristics of bidirection scans as a function of UV irradiation time: (a) the devices with the $AzoC6CF_3$-Au-NPs substrates, (b) the devices with the $AzoC6CH_3$-Au-NPs substrates.

in both directions along with scan range increase in both directions, indicating both holes and electrons can be trapped in the Au-NPs. Nevertheless, a rather asymmetric shift was obtained for the $AzoC_6CF_3$-Au-NP device, the initial transfer curves (from +20 V to −20 V) shifted to positive direction faster than to negative direction with the same increase in scan ranges. This suggests negative charges are trapped faster with the $AzoC_6CF_3$-Au-NPs than positive charges do.

3.2.3. Effect of Chain Length. The IV hysteresis of the device with Au-NPs covered by CF_3-substituted azobenzene at the surface through alkyl chains of different lengths, abbreviated as $AzoC_{10}CF_3$, $AzoC_6CF_3$ and $AzoC_2CF_3$, are compared (Figure 6). In spite of the similar work function of Au substrates modified with these CF_3-substituted azobenzenes (Table 1), the memory window increased with decreasing length of the tethering chain. The largest hysteresis in positive direction and the highest source-drain current were observed in the $AzoC_2CF_3$-Au-NP system, even though the crystallinity of the pentacene film decreased slightly in this system (judging from the intensity of the (001) diffraction peaks). The limiting ON or OFF currents were not reached after 180 s for all three systems. Yet the shortest tethering chain gave the largest current change and thus the largest ON/OFF ratio (Figure 7a). Apparently a longer chain suppresses the amount of charges that can be trapped under the same gate bias. Yet for the same reason, a longer retention time is extrapolated for longer chain length (Figure 7b). For $AzoC_2CF_3$-Au-NPs, the retention time is apparently longer than that for C10-Au-NPs (where a C10 chain has a similar chain length as the $AzoC_2CF_3$ molecule), although the work function of Au-NPs covered with $AzoC_2CF_3$ increased, disfavoring charge trapping. This confirms that the azobenzene monolayer plays a critical role on the retention property of the Au-NP devices.

3.2.4. Effect of UV Irradiation. Although cis−trans isomerization of azobenzene moiety by photo irradiation can result in large molecular dipole moment change, which may modulate the threshold voltage,[42] our previous work showed that UV-irradiation of an azobenzene SAM on a planar substrate modulates the threshold voltage by charge transfer between the excited state of azobenzene moieties and the pentacene molecules.[41] For $AzoC6CF_3$-Au-NP devices, a larger hysteresis with a positive threshold voltage shift was observed depending on the length of UV irradiation. The source-drain current increased with increasing irradiating time as well (Figure 8a). These could be attributed to electrons transfer from the HOMO of pentacene to the HOMO of photoexcited $AzoC6CF_3$-Au-NPs, so that more positive charge carriers generated at the pentacene layer, leading to threshold voltage shift in the positive direction and higher source−drain current. Photoisomerization of the azobenzene moieties can be excluded because the trans−cis isomerization upon UV-irradiation would result in diminishing of the interfacial dipoles and a threshold voltage shift in the negative direction is expected, which is contrary to the observation.[41] However, a longer UV irradiation induced a larger hysteresis in which threshold voltage shift toward the negative direction and a smaller source-drain current in the case of $AzoC6CH_3$-Au-NP devices, attributable to electron transfer from excited $AzoC6CH_3$ moieties to the HOMO of pentacene, with the positively charged $AzoCH_3$-Au-NPs causing a negative threshold voltage shift and decreased source−drain current (Figure 8b). These results indicated the memory window (threshold voltage shift) and source−drain current can be changed by the

dx.doi.org/10.1021/am4023253 | ACS Appl. Mater. Interfaces 2013, 5, 9528−9536

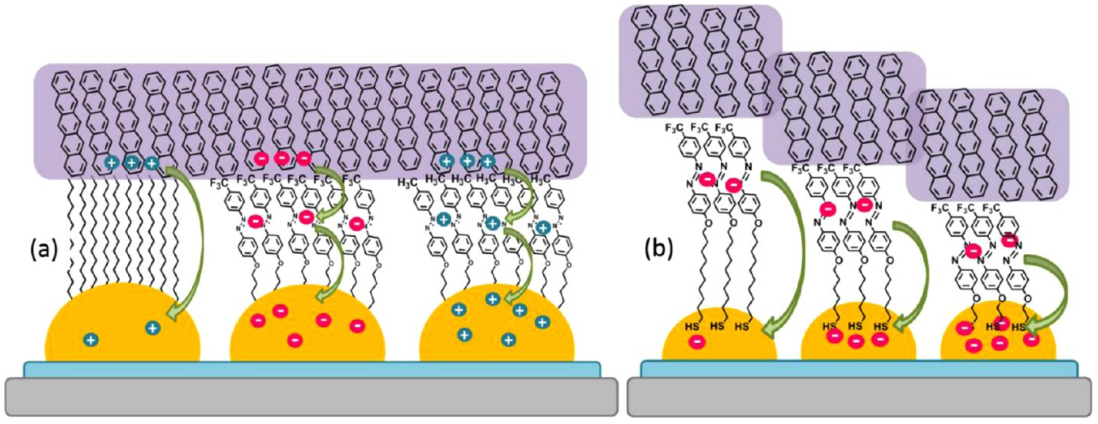

Figure 9. Schematic diagram showing the charge trapping process in variously functionalized Au-NPs in the pentacene-based transistor/memory devices.

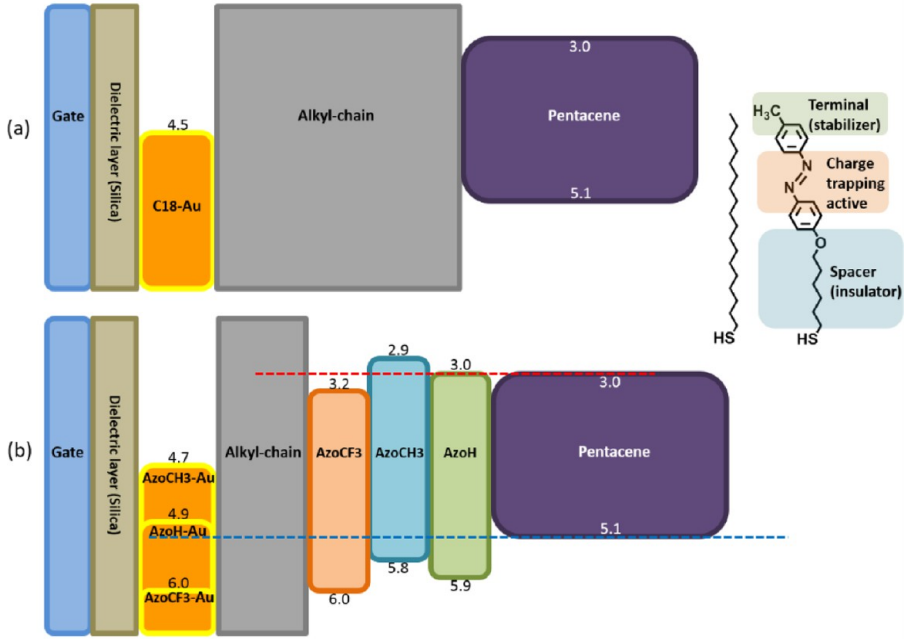

Figure 10. Energy-band diagram in zero-gate-voltage configuration of (a) C18-covered Au NP device, and (b) various azobenzene-modified Au NP devices.

photo irradiation, because of the opposite charge trapping, which in turn strongly depends on the nature of the substituent in azobenzene moieties.

3.3. Mechanistic Interpretation. The observations above are explained with a general picture (Figure 9) and the corresponding energy level alignments in the system (Figure 10). When Au-NPs (or other vehicles that can accommodate charges) are embedded in the conducting channel of the transistor at the semiconductor/dielectric interface, the charge carriers can get in and out of the Au-NPs, depending on the Schottky barrier existing between the frontier orbitals of the semiconductor and the Fermi level of the Au metal. The hole carriers accumulated at the pentacene molecules under a negative gate bias can be trapped into the Au-NPs because the HOMO energy level (~5.1 eV) of pentacene is of similar level as the Fermi level of Au (5.0 eV). However, the charges can also migrate out (detrapped) from the Au-NPs when the gate bias is removed. When a self-assembled monolayer (SAM) of *n*-alkanethiol is adsorbed on the Au-NP surface, it serves as a barrier not only for charges to detrap from the NPs but also a barrier for charges to be trapped into the particles. It was demonstrated earlier that a longer alkyl chain poses a larger barrier for trapping the charges than a shorter chain, thus more charges will be trapped and thus larger hysteresis will result for the shorter alkyl chain modified Au-NPs, when the same gate pulse was applied.[36,23] With azobenzene-carrying SAM, a mediating layer is provided due to the oxidizable group of azobenzenes. With $AzoC_6CH_3$–Au-NPs, where a similar chain length and dipole direction as in C18–Au–NPs, more charges are trapped and larger hysteresis is obtained. Besides trapping charges itself, the $AzoC_6CH_3$ moieties also mediate and facilitate the trapping of hole carriers into the Au-NPs because the positive charges may reside on the azobenzene moieties and then transport to the NPs. When comparing the effect of substituents, the $AzoC_6CF_3$-Au-NPs showed smaller hysteresis because the destabilizing effect of CF_3 for positive charge and possibly the larger work function of the $AzoC_6CF_3$-modified Au substrate, both of which will reduce the amount of hole carriers

dx.doi.org/10.1021/am4023253 | ACS Appl. Mater. Interfaces 2013, 5, 9528–9536

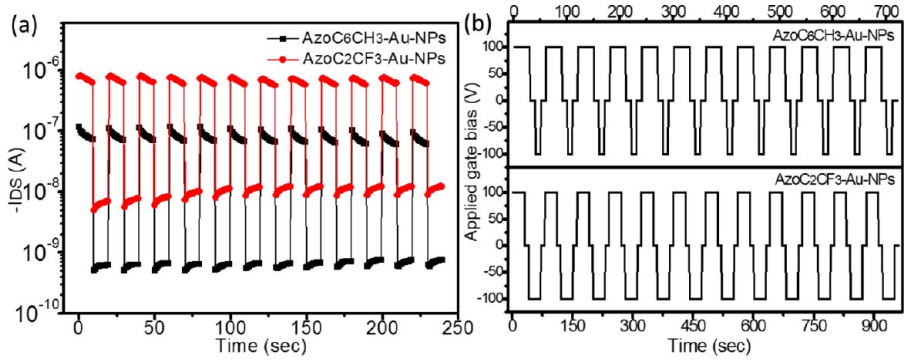

Figure 11. (a) Reversible switching between ON- and OFF- states of the devices with $AzoC_6CH_3$-Au-NPs and $AzoC_2CF_3$-Au-NPs, respectively; (b) the corresponding pulse sequence for the measurement.

that can transport to the Au-NPs. When the source−drain currents as a function of gate pulse time are compared, it is noted that the C18-Au-NP device did not reach its maximum current (ON state) or minimum current (OFF state) even after 180 s, whereas the $AzoC_6CH_3$-Au-NP device reached the "OFF" state in 0.01 s. The fast response time is believed to be due to the stabilizing effect of CH_3 groups for the positive charge so that the group mediate the hole carrier trapping effectively. The "ON" state is reached slower, after the positive gate pulse of 60 s. This is due to the less effective mediating effect of $AzoC_6CH_3$ group for negative charge under the positive gate bias. But it is still faster than the C18−Au−NPs, where no mediating group is present. For the $AzoC_6CF_3$−Au-NPs system, the OFF state is reached slower because the CF_3-substituted azobenzene is less effective in mediating the positive charges to the Au-NPs. The "ON" state is reached faster than other systems because upon positive gate pulse, the negative charges are mediated by the CF_3-substituted azobenzene moieties. Finally, the $AzoC_6CH_3$-Au-NPs system has much longer retention time (or slower relaxation of currents) than the other systems after the same gate pulse time. This is attributed to the more charge carriers stored in the $AzoC_6CH_3$-Au-NPs system as a result of efficient mediating effect of $AzoC_6CH_3$ groups. A shell of stabilized charged $AzoC_6CH_3$ layer surrounding the Au-NPs also may slow down the de-trapping of the carriers in the particles so that a longer retention time was observed.

The reversible switching of the $AzoC_6CH_3$-Au-NP device and $AzoC_2CF_3$-Au-NP device were demonstrated by the write-read-erase-read (WRER) cycles, respectively, as shown in Figure 11. Reading was carried out by measuring the drain current without any applied gate bias. The writing and erasing processes were at the gate bias of −100 V/100 V for 10 and 30 s for the $AzoC_6CH_3$−Au-NP device, and −100 V/100 V for 30 s for the $AzoC_2CF_3$-Au-NP device, respectively. The responding "ON" and "OFF" currents of the devices could be well-separated and maintained over repeating cycles. The reliability and reversibility of the current switching suggest the potential applications of these systems for nonvolatile flash type memory.

4. CONCLUSIONS

In conclusion, we demonstrated that by covering gold nanoparticle surfaces with azobenzene moieties allows for fast charge trapping and extended charge retaining in the Au-NPs, which serve as a floating gate in the pentacene-based transistor. The azobenzene moieties provide additional trapping sites than the purely insulating alkyl chains. These azobenzene moieties also mediate the trapping of charged carriers into the nanoparticles and improve the response time of charge trapping (or the programing) process. The substituent on the azobenzene further modulates the efficiency of charge trapping. Retention of the charges can also be improved because the stabilized charged outer layer of azobenzene can shield the charges in the nanoparticles from escaping. Thus the incorporation of the azobenzene moieties at the surface would impart a fast response and extended retention of the conductivity switching.

■ ASSOCIATED CONTENT

Ⓢ Supporting Information

The synthetic procedure and characterization data for all azobenzene-carrying thiols, the reflection−absorption infrared spectra measured for various SAM-modified Au surfaces, and the AFM images of thermally evaporating 4 nm pure gold metal onto the silica substrate. This material is available free of charge via the Internet at http://pubs.acs.org.

■ AUTHOR INFORMATION

Corresponding Author

*E-mail: ytt@chem.sionica.edu.tw.

Notes

The authors declare no competing financial interest.

■ ACKNOWLEDGMENTS

The authors thank the National Science Council of Taiwan, the Republic of China (Grant 101-2113-M-001-006-MY3), and Academia Sinica for financial support of this work.

■ REFERENCES

(1) Gelinck, G.; Heremans, P.; Nomoto, K.; Anthopoulos, T. D. *Adv. Mater.* **2010**, *22*, 3778−3798.
(2) Moonen, P. F.; Yakimets, I.; Huskens, J. *Adv. Mater.* **2012**, *24*, 5526−5541.
(3) Carlson, A.; Bowen, A. M.; Huang, Y.; Nuzzo, R. G.; Rogers, J. A. *Adv. Mater.* **2012**, *24*, 5284−5318.
(4) Wang, C.; Dong, H.; Hu, W.; Liu, Y.; Zhu, D. *Chem. Rev.* **2012**, *112*, 2208−2267.
(5) Scott, J. C.; Bozano, L. D. *Adv. Mater.* **2007**, *19*, 1452−1463.
(6) Cho, B.; Song, S.; Ji, Y.; Kim, T. W.; Lee, T. *Adv. Funct. Mater.* **2011**, *21*, 2806−2829.
(7) Kim, T. W.; Yang, Y.; Li, F.; Kwan, W. L. *NPG Asia Mater.* **2012**, *4*, e18.
(8) Guo, Y.; Yu, G.; Liu, Y. *Adv. Mater.* **2010**, *22*, 4427−4447.
(9) Di, C. A.; Zhang, F.; Zhu, D. *Adv. Mater.* **2013**, *25*, 313−330.

(10) Bertolazzi, S.; Krasnozhon, D.; Kis, A. *ACS Nano* **2013**, *7*, 3246−3252.
(11) Tseng, C. W.; Tao, Y. T. *ACS Appl. Mater. Interfaces* **2010**, *2*, 3231−3240.
(12) Kim, S. M.; Song, E. B.; Lee, S.; Zhu, J.; Seo, D. H.; Mecklenburg, M.; Seo, S.; Wang, K. L. *ACS Nano* **2012**, *6*, 7879−7884.
(13) Dao, T. T.; Matsushima, T.; Murata, H. *Org. Electron.* **2012**, *13*, 2709−2715.
(14) Leong, W. L.; Mathews, N.; Tan, B.; Vaidyanathan, S.; Dötzb, F.; Mhaisalkar, S. *J. Mater. Chem.* **2011**, *21*, 5203−5214.
(15) Baeg, K. J.; Khim, D.; Kim, J.; Yang, B. D.; Kang, M.; Jung, S. W.; You, I. K.; Kim, D. Y.; Noh, Y. Y. *Adv. Funct. Mater.* **2012**, *22*, 2915−2926.
(16) Chou, Y. H.; Yen, H. J.; Tsai, C. L.; Lee, W. Y.; Liou, G. S.; Chen, W. C. *J. Mater. Chem. C* **2013**, *1*, 3235−3243.
(17) Tripathi, A. K.; Breemen, A. J. J. M. V.; Shen, J.; Gao, Q.; Ivan, M. G.; Reimann, K.; Meinders, E. R.; Gelinck, G. H. *Adv. Mater.* **2011**, *23*, 4146−4151.
(18) Khan, M. A.; Bhansali, U. S.; Alshareef, H. N. *Adv. Mater.* **2012**, *24*, 2165−2170.
(19) Hwang, S. K.; Bae, I.; Kim, R. H.; Park, C. *Adv. Mater.* **2012**, *24*, 5910−5914.
(20) Kang, M.; Baeg, K. J.; Khim, D.; Noh, Y. Y.; Kim, D. Y. *Adv. Funct. Mater.* **2013**, *23*, 3503−3512.
(21) Zhou, Y.; Han, S. T.; Xu, Z. X.; Roy, V. A. L. *Adv. Mater.* **2012**, *24*, 1247−1251.
(22) Wei, Q.; Lin, Y.; Anderson, E. R.; Briseno, A. L.; Gido, S. P.; Watkins, J. J. *ACS Nano* **2012**, *6*, 1188−1194.
(23) Tseng, C. W.; Chen, Y. L.; Tao, Y. T. *Org. Electron.* **2012**, *13*, 1436−1442.
(24) Han, S. T.; Zhou, Y.; Xu, Z. X.; Huang, L. B.; Yang, X. B.; Roy, V. A. L. *Adv. Mater.* **2012**, *24*, 3556−3561.
(25) Chang, H. C.; Lee, W. Y.; Tai, Y.; Wu, K. W.; Chen, W. C. *Nanoscale* **2012**, *4*, 6629−6636.
(26) Kay, E. R.; Leigh, D. A.; Zerbetto, F. *Angew. Chem., Int. Ed.* **2007**, *46*, 72−191.
(27) Spinks, G. M. *Angew. Chem., Int. Ed.* **2012**, *51*, 2285−2287.
(28) Crivillers, N.; Orgiu, E.; Reinders, F.; Mayor, M.; Samorì, P. *Adv. Mater.* **2011**, *23*, 1447−1452.
(29) Cao, Y.; Dong, S.; Liu, S.; Liu, Z.; Guo, X. *Angew. Chem., Int. Ed.* **2013**, *52*, 3906−3910.
(30) Kim, M.; Safron, N. S.; Huang, C.; Arnold, M. S.; Gopalan, P. *Nano Lett.* **2012**, *12*, 182−187.
(31) Peimyoo, N.; Li, J.; Shang, J.; Shen, X.; Qiu, C.; Xie, L.; Huang, W.; Yu, T. *ACS Nano* **2012**, *6*, 8878−8886.
(32) Wang, S. Y.; Huang, D. C. H.; Tao, Y. T. *J. Chin. Chem. Soc.* **2012**, *59*, 9−17.
(33) Crispin, X.; Geskin, V.; Crispin, A.; Cornil, J.; Lazzaroni, R.; Salaneck, W. R.; Bredas, J. L. *J. Am. Chem. Soc.* **2002**, *124*, 8131−8141.
(34) Boer, B. D.; Hadipour, A.; Mandoc, M. M.; Woudenbergh, T. V.; Blom, P. W. M. *Adv. Mater.* **2005**, *17*, 621−625.
(35) Hu, W. S.; Tao, Y. T.; Hsu, Y. J.; Wei, D. H.; Wu, Y. S. *Langmuir* **2005**, *21*, 2260−2266.
(36) Nayak, P. K.; Kim, J.; Cho, J.; Lee, C.; Hong, Y. *Langmuir* **2009**, *25*, 6565−6569.
(37) Tseng, C. W.; Tao, Y. T. *J. Am. Chem. Soc.* **2009**, *131*, 12441−12450.
(38) Chen, C. M.; Liu, C. M.; Wei, K. H.; Jeng, U. S.; Su, C. H. *J. Mater. Chem.* **2012**, *22*, 454−461.
(39) Han, S. T.; Zhou, Y.; Wang, C.; He, L.; Zhang, W.; Roy, V. A. L. *Adv. Mater.* **2013**, *25*, 872−877.
(40) Baeg, K. J.; Noh, Y. Y.; Sirringhaus, H.; Kim, D. Y. *Adv. Funct. Mater.* **2010**, *20*, 224−230.
(41) Tseng, C. W.; Huang, D. C.; Tao, Y. T. *ACS Appl. Mater. Interfaces* **2012**, *4*, 5483−5491.
(42) Paoprasert, P.; Park, B.; Kim, H.; Colavita, P.; Hamers, R. J.; Evans, P. G.; Gopalan, P. *Adv. Mater.* **2008**, *20*, 4180−4184.